PHYSICAL REVIEW A **80**, 052709 (2009)

Electron-scattering cross sections for collisions with tetrahydrofuran from 50 to 5000 eV

M. Fuss,[1] A. Muñoz,[2] J. C. Oller,[2] F. Blanco,[3] D. Almeida,[4] P. Limão-Vieira,[4] T. P. D. Do,[5] M. J. Brunger,[5] and G. García[1,6]
[1]*Instituto de Matemáticas y Física Fundamental, Consejo Superior de Investigaciones Científicas (CSIC), Serrano 113-bis, 28006 Madrid, Spain*
[2]*Centro de Investigaciones Energéticas, Medioambientales y Tecnológicas (CIEMAT), Avenida Complutense 22, 28040 Madrid, Spain*
[3]*Departamento de Física Atómica, Molecular y Nuclear, Universidad Complutense de Madrid, Avenida Complutense s.n., 28040 Madrid, Spain*
[4]*Departamento de Física, CEFITEC, Universidade Nova de Lisboa, 2829-516 Caparica, Portugal*
[5]*ARC Centre for Antimatter-Matter Studies, School of Chemistry, Physics and Earth Sciences, Flinders University, G.P.O. Box 2100, Adelaide, South Australia 5001, Australia*
[6]*Departamento de Física de los Materiales, UNED, Senda de Rey 9, 28040 Madrid, Spain*
(Received 16 September 2009; published 19 November 2009)

In this paper, we report on total electron tetrahydrofuran (C_4H_8O) scattering cross-section measurements for energies in the range from 50 to 5000 eV with experimental errors of about 5%. In addition, integral elastic and inelastic cross sections have been calculated over a broad energy range (1–10 000 eV), with an optical potential method assuming a screening-corrected independent atom representation. Partial and total ionization cross sections have been also obtained by combining simultaneous electron and ion measurements with a time-of-flight analysis of the ionic induced fragmentation. Finally, an average energy distribution of secondary electrons has been derived from these measurements in order to provide data for modeling electron-induced damage in biomolecular systems.

DOI: 10.1103/PhysRevA.80.052709 PACS number(s): 34.80.Bm, 34.80.Gs, 34.50.Bw

I. INTRODUCTION

Radiation damage in biomolecular systems has been extensively studied in the last decade, paying special attention to the role of secondary electrons [1–3] in radiation induced effects. The main purpose for some of these studies is to provide radiation interaction models to be used in biomedical applications, both for diagnosis and therapy. These models require electron-scattering cross sections over a wide energy range, in principle, from the high energy of the primary radiation slowing down to thermal energies. Although these parameters have been widely studied for different atomic and molecular targets [4–6], most of the works have been restricted to the low energy domain. Indeed, from the experimental point of view, electron-scattering cross-section data for energies above 500 eV are scarce. Concerning calculations, a complete scattering treatment is not affordable at all these energies and so some approximations are required. For high energies, it is customary to use the first Born approximation to calculate cross-section data, both for elastic and inelastic scatterings. However, we have previously shown [7–10] that this approximation overestimates cross-section values for simple life-relevant molecules even at a 5000 eV incident electron energy. At intermediate and high energies (50–5000 eV), optical potential calculations, assuming an independent atom configuration, have proven to be a simple and powerful tool [11–13] applicable to different-sized molecules, from diatomic molecules to complex biomolecules (DNA and RNA bases [14] or DNA dodecamer complex [15]) when appropriate corrections are included [15].

One of the most important molecules for biological systems is water. Consequently, electrons interacting with H_2O molecules have been studied, both theoretically and experimentally, by means of many different techniques. We have recently published a detailed study of electron-scattering cross sections from water molecules [16], including comparisons to previous results and available review papers [17,18]. Going to more complex biomolecules, tetrahydrofuran-C_4H_8O (THF) reveals great interest due to its similar structure to that of the sugar components of DNA and RNA [19]. As a consequence, electron-scattering cross sections by THF have been measured and calculated in the last few years for intermediate and low energies [19–30]. However, for energies above 500 eV, experimental and theoretical electron interaction data are almost nonexistent for this molecule.

These considerations partly motivated the present study, in which absolute experimental electron-scattering total cross sections (TCSs) have been determined by measuring the attenuation of an electron beam through a sample of THF for energies between 50 and 5000 eV. Differential and integral electron-scattering cross sections have also been calculated by using an optical potential method, based on an independent atom representation but including screening corrections in order to emulate the molecular structure. In addition, partial and total electron-impact ionization cross sections have been measured with a pulsed crossed-beam technique in combination with a time-of-flight analysis of the induced molecular fragmentation.

Other important information in simulations to define single-particle tracks includes the energy-loss distribution function and the energy distribution of the secondary electrons. As a complement of the abovementioned experiments, we will provide these distribution functions as derived from direct measurements of the primary electron energy-loss spectra or energy analysis of the produced secondary electrons, respectively.

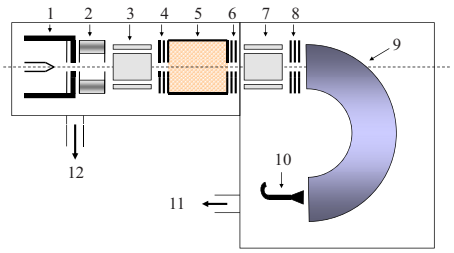

FIG. 1. (Color online) Present experimental apparatus: 1, electron gun; 2, transverse magnetic field; 3 and 7, quadrupole electrostatic plates; 4, 6, and 8, decelerating and accelerating lenses; 5, scattering chamber; 9, hemispherical electrostatic energy analyzer; 10, channel electron multiplier; 11 and 12 vacuum turbo molecular pumps.

II. MEASUREMENTS

The experimental configuration to measure TCS and energy-loss spectra was based on that previously reported [16]. However, in contrast with the procedure used in [16], ionization cross sections have now also been measured in an independent system. Here, we will only thus describe briefly the original apparatus, giving more details about the system which was used to determine the partial and total ionization cross sections and the energy distribution of the secondary electrons.

A schematic diagram of the first system is shown in Fig. 1. The primary electron beam was produced by an emitting filament. Thereafter, a combination of magnetic and electrostatic fields controls the direction of the beam and reduces the energy spread to ~100 meV. The collision chamber containing the gas target was a stainless-steel tube delineated by two apertures. The entrance aperture was always 0.5 mm in diameter, whereas different exit apertures with 1, 2, or 3 mm diameter, as well as two different lengths of the collision chamber of 10 and 50 mm, respectively, were used according to the experimental requirements. The gas pressure in the chamber was measured with an absolute capacitance gauge (MKS Baratron 127A) and it was varied from 0.1 to 10 mTorr according to the experimental conditions. Electrons emerging from the collision chamber were deflected by a quadrupole electrostatic system to select the angle of analysis. The energy analyzer was a hemispherical electrostatic spectrometer in combination with a retarding field. In these conditions, the energy resolution of the spectrometer was about 0.5 eV (full width at half maximum, FWHM) for the whole energy range considered here. Transmitted electrons through the analyzer were finally detected by a channel electron multiplier operating in single pulse counting mode. Count rates were typically on the order of 10^3 s^{-1} for the total cross-section measurements and up to 10^4 s^{-1} through the energy-loss spectra determination. Note that he maximum angular acceptance of the energy analyzer was 1.9×10^{-5} sr. The whole system was differentially pumped by two turbo pumps of 80 and 250 l/s, respectively, reaching a background pressure of $\sim 10^{-8}$ Torr. On the other hand, the pressure in the electron gun and energy analyzer region was maintained lower than 10^{-6} Torr during the measurements.

TCSs have been measured for energies between 50 and 5000 eV, while energy-loss spectra were measured in the same energy range but for different scattering angles. These angles were selected by deflecting the scattered beam with a quadrupole electrostatic plate system. A typical energy-loss spectrum for 1000 eV incident energy, 10 mTorr pressure in the gas cell, and an analysis angle around 10° is shown in Fig. 2.

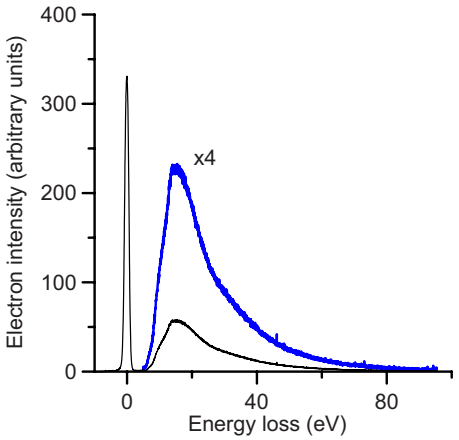

FIG. 2. (Color online) Typical measured electron energy-loss spectrum for a 1000 eV incident energy electron beam. In this case, there was 10 mTorr pressure in the gas cell and a 10° analysis angle.

The second experimental system is schematically shown in Fig. 3. The electron gun consists of an emitting filament, extractive and focusing electrodes, and an electrostatic quadrupole system to drive the beam into the collision chamber. The collision chamber is a gas cell which is limited along the direction of the electron beam by two apertures of 0.5 and 2 mm diameter, respectively, separated by 30 mm. Another two apertures of 2 mm diameter are placed perpendicular to both

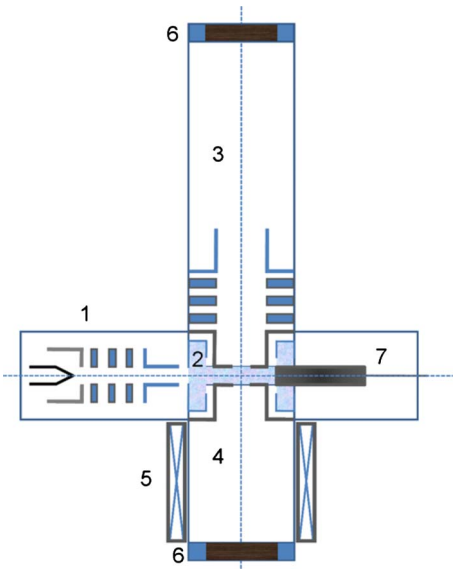

FIG. 3. (Color online) Experimental system to determine total and partial ionization cross sections by electron impact: 1, electron gun (filament, control electrode focusing lens, and deflecting plates); 2, gas cell; 3, ion drift tube (extracting electrode, focusing lens, and deflecting plates); 4, electron drift tube; 5, magnetic coils; 6, microchannel plate detectors; 7, Faraday cup.

sides of the incident beam and are separated by 3 mm. These four apertures define the geometry of the collision region, in which the target gas is introduced by a needle valve at a well-known pressure controlled by a MKS Baratron capacitance gauge. Note that each perpendicular aperture defines the entrance of a differentially pumped drift tube. The larger drift tube (1.5 m length) drives the collected ion beam by means of two additional apertures, 3 mm in diameter, and an electrostatic quadrupole system which controls the ion direction. These ions are finally detected by a two-stage microchannel plate assembly operating in a single pulse mode. The other drift tube, with a geometrical length of 0.5 m, transports and detects the extracted secondary electrons. A variable parallel magnetic field (0–0.01 T) is externally applied to increase the actual length of these electron trajectories. As for the ions, the secondary electrons are detected by a two-stage microchannel detector in single-pulse operation mode.

The primary electron beam in this second system was pulsed by applying a +10 V train of pulses to the gun control electrode, each of 10^{-5} s duration and having a repetition rate of 10^4 Hz. Extractive bipolar pulses of variable amplitude, up to ± 400 V, in synchronism with the electron-beam pulses, were applied to the perpendicular apertures. Under these conditions, ions and secondary electrons are extracted in opposite directions toward the respective drift tubes. The secondary electron and ion signals were independently stored as a function of time by a two-channel Tektronix TDS3032C digital scope. Primary electrons, transmitted through the gas cell, are detected by a Faraday cup. Note that the average electron currents in the cup, typically on the order of 10^{-8} A, were measured with a Keithley 6517A electrometer. Total ion intensity measurements, normalized by the primary electron currents at each measured electron energy, provided relative total ionization cross sections as a function of electron energies from 50 to 5000 eV. For a given energy, partial cross sections (corresponding to the different observed ion fragmentation channels) were determined from the consequent time-of-flight spectra provided by the ion drift tube. These relative values were put on an absolute scale by normalizing to the electron-impact ionization cross section for N_2 at 1000 eV, which was assumed to be $(0.85 \pm 0.05) \times 10^{-16}$ cm^2 in accordance with previous measurements available in the literature [31–35]. Similarly, secondary electron distribution energies were derived from time-of-flight measurements given by the electron drift tube.

III. CALCULATIONS

The optical potential method described in previous papers [10–12] has been used to calculate differential and integral elastic, as well as integral inelastic, electron-THF scattering cross sections. This calculation includes the recent adjustments we have introduced in the potential which significantly improved results for many molecular targets, both for the integral [12] and differential [13] cross sections, especially in the low energy region. Processes involving nuclear motion are neglected in this calculation. The present method considers inelastic scattering as being due to electron-electron interaction processes; only those arising from electronic excitation are considered, thus rotational and vibrational excitations are ignored. This restriction is not thought to be significant in general for the relatively high energies considered in this study.

Following the above procedures, we present calculated integral electron-scattering cross sections (elastic, inelastic, and total) from 1 to 10 000 eV. The reliability of these results, in comparison to the experimental data, is discussed in the next section.

TABLE I. Experimental and theoretical electron-scattering cross sections (10^{-16} cm^2) for THF as obtained in this study.

	Calculation (10^{-16} cm^2)			Experiment (10^{-16} cm^2)	
Energy (eV)	Elastic (σ_{el})	Inelastic (σ_{inel})	Total (σ_{tot})	Ionization (σ_{ion})	Total (σ_{tot})
1	79.5		79.5		
1.5	74.2		74.2		
2	68.6		68.6		
3	58.5		58.5		
4	54.6		54.6		
5	51.8		51.8		
7	47.3		47.3		
10	43.1	0.07	43.2		
15	37.2	2.97	40.3		
20	31.1	7.84	38.9		
30	23.0	14.2	37.2		
40	19.2	16.2	37.2		
50	16.8	16.6	33.3	11.2	44.2
70	13.9	16.2	30.2		36.5
100	11.5	14.8	26.3	12.5	31.4
150	9.27	12.7	22.0	12.0	26.3
200	7.90	11.1	19.1	9.89	22.0
300	6.19	9.04	15.2	7.90	16.6
400	5.15	7.59	12.8	6.57	13.7
500	4.45	6.61	11.1	5.64	11.8
700	3.53	5.24	8.76		9.08
1000	2.70	4.03	6.72	3.39	6.96
1500	1.95	2.91	4.86	2.49	5.11
2000	1.54	2.30	3.84	1.99	3.90
3000	1.09	1.63	2.72	1.46	2.84
4000	0.851	1.27	2.12	1.16	2.17
5000	0.700	1.04	1.74	0.978	1.78
7000	0.518	0.770	1.29		
10000	0.378	0.557	0.932		

IV. RESULTS AND DISCUSSION

TCSs measured in this study, from 50 to 5000 eV, are shown in Table I and plotted in Fig. 4. The estimated experimental errors on these data are less than 5% (see Ref. [36] for a detailed analysis of the main error sources). Previous

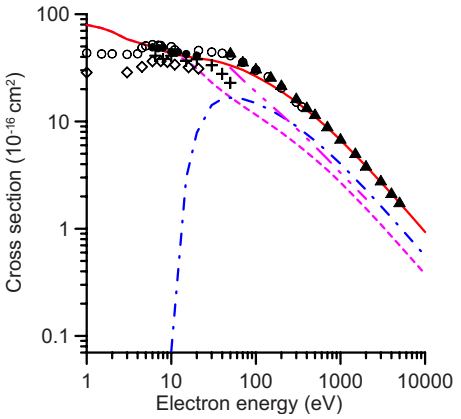

FIG. 4. (Color online) Cross section for electron scattering by THF: ▲, present experimental total cross sections; ○, experimental total cross-section data from Ref. [22]; ◇, experimental total cross sections given in Ref. [21]; —, present total cross-section calculation; -··-, present inelastic cross-section calculation; —, present elastic cross-section calculation; -···-, elastic cross section calculated in Ref. [37]; +, experimental elastic cross section from Ref. [23]; ●, experimental elastic cross sections from Ref. [24].

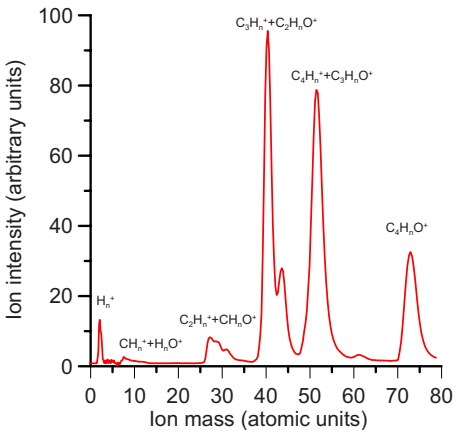

FIG. 5. (Color online) Ion fragment mass spectrum derived from the time-of-flight spectrum for an incident electron energy of 1000 eV. Species detected are as labeled on the figure.

measurements available in the literature [21,22] are also included in this figure for comparison. As shown in Fig. 4, there is good agreement, within experimental error, between the present data and those of Ref. [22], reaching a maximum difference of 9% at 400 eV. Low energy data from [21] are systematically lower than those of [22], but showing a similar energy dependence. This discrepancy is due to the poorer angular resolution of the apparatus used in [21] compared to that of [22]. Correcting for this effect, by using the differential cross sections measured in [23], the data of Ref. [21] increase by up to about 40% being therefore now in satisfactory agreement with those of [22].

Regarding the theoretical data, Table I also includes our calculated integral elastic and integral inelastic (absorption potential contribution) cross sections. As may be seen in Fig. 4, the total theoretical electron-scattering cross sections, obtained by adding those partial cross sections, show excellent agreement with our experimental data in the overlapping energy region (50–5000 eV). However, integral elastic cross-section calculations from Mozejko and Sanche [37], obtained with an independent atom model, show important discrepancies with the present results, being 23% higher than ours at 2000 eV and increasing up to 88% larger at 50 eV. The origin of this discrepancy is unclear; we have shown that our screening correction [14] improves significantly the independent atom calculation results for relatively low energies. Nonetheless, this does not explain the ~20% discrepancy at 2000 eV.

Below 50 eV, we would expect our method to become less reliable as energy further decreases. However, as may be seen in Fig. 4, recent measurements carried out by Colyer *et al.* [23] and Dampc *et al.* [24,25] show reasonable agreement with our calculated integral elastic cross sections even at energies as low as around 10 eV.

Concerning our ionization cross-section data, Fig. 5 represents a typical ion mass spectrum derived from the time-of-flight spectrum showing the ion fragmentation pattern for an incident electron energy of 1000 eV. As can be seen, our mass resolution is somewhat limited, so that fragments differing only by one mass unit are not fully resolved. Notwithstanding that point, present partial and total ionization cross-section results from our measurements between 50 and 5000 eV are shown in Fig. 6 and Table II. Experimental errors for the total ionization data, including the accuracy of the present normalizing procedure, have been estimated at about 7%. For the partial cross sections, the statistical uncertainties tend to be higher for the less abundant fragments, reaching a maximum value of ~15% for the H_n^+ ($n=1,2$) ionic fragments. As can be seen in Fig. 6, our absolute total ionization data show excellent agreement, to within 6%, with the calculations of Ref. [37] derived with the binary-encounter-Bethe (BEB) model.

When modeling radiation effects at the molecular level, an energy distribution of the generated secondary electrons is needed at each energy of the primary ionizing radiation. As mentioned earlier, time-of-flight measurements of secondary electrons produced by ionization of the target provide such

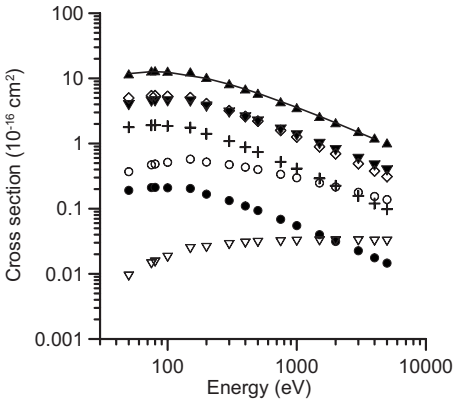

FIG. 6. Total and partial electron-impact ionization cross sections in THF. ▲, present total ionization cross-section measurements; —, total ionization cross sections calculated in Ref. [37]. Present partial ionization cross sections corresponding to: ▽, H_n^+; ●, CH_n^++H_nO^+; ○, $C_2H_n^+$+CH_nO^+; ▼, $C_3H_n^+$+$C_2H_nO^+$; ◇, $C_4H_n^+$+$C_3H_nO^+$; +, $C_4H_nO^+$.

TABLE II. Total and partial experimental electron-impact ionization cross sections (10^{-16} cm^2) in THF.

	Cross section (10^{-16} cm^2)						
Energy (eV)	H_n^+	CH_n^++H_nO^+	$C_2H_n^+$+CH_nO^+	$C_3H_n^+$+$C_2H_nO^+$	$C_4H_n^+$+$C_3H_nO^+$	$C_4H_nO^+$	Total (σ_{ion})
50	0.191	0.0092	0.370	3.88	4.99	1.78	11.2
75	0.211	0.0142	0.470	4.39	5.42	1.91	12.4
80	0.212	0.0151	0.484	4.43	5.44	1.92	12.5
100	0.209	0.0179	0.515	4.43	5.31	1.86	12.3
150	0.204	0.0243	0.575	4.4	5.07	1.76	12.0
200	0.167	0.0253	0.520	3.67	4.10	1.41	9.89
300	0.133	0.0280	0.475	2.98	3.20	1.09	7.90
400	0.11	0.0295	0.434	2.51	2.61	0.881	6.57
500	0.0937	0.0303	0.400	2.17	2.21	0.741	5.64
750	0.0687	0.0310	0.337	1.63	1.59	0.523	4.18
1000	0.0550	0.0315	0.298	1.33	1.26	0.414	3.39
1500	0.0399	0.0319	0.248	0.984	0.895	0.292	2.49
2000	0.0314	0.0319	0.216	0.789	0.696	0.225	1.99
3000	0.0226	0.0320	0.178	0.580	0.491	0.157	1.46
4000	0.0176	0.0317	0.154	0.460	0.378	0.120	1.16
5000	0.0146	0.0316	0.138	0.386	0.310	0.0981	0.978

an energy distribution at each energy. In practice, however, this represents an enormous amount of data to incorporate into the simulation so that usually an average distribution is employed. This average distribution is formed by averaging our measured energy distributions for impact energies from 100 to 5000 eV, with the resultant distribution function being plotted in Fig. 7. Note that our electron time-of-flight measurements have been calibrated by using a simple electron gun with 500 meV energy spread. We can therefore expect that the accuracy on the absolute values of our electron energies must be within 10%. As shown in this figure, we find that the most probable secondary electron energies are at around 4 eV, with a resultant average energy of 14.8 ± 1.5 eV for our measured distributions.

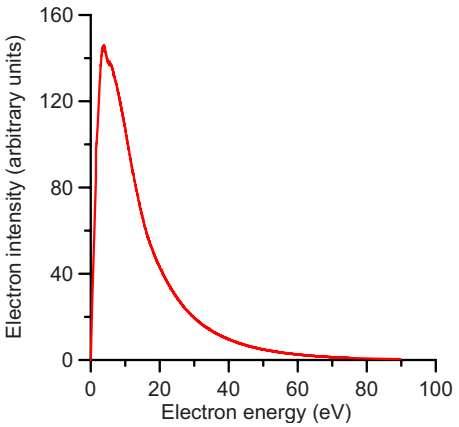

FIG. 7. (Color online) Average energy distribution of secondary electrons for incident electron energies above 100 eV.

V. CONCLUSIONS

In this study, we presented accurate experimental cross sections for total electron scattering and total electron-impact ionization of THF from 50 to 5000 eV. These data are relevant parameters for radiation-based biomedical applications and in particular to get benchmark parameters for electron-induced damage in biomolecular systems. Note that the present total cross-section data are the first measurements for energies above 350 eV. Below this energy, previous measurements [21,22] show good agreement with the present data. Furthermore, these measurements confirm that our screened corrected model potential calculation, for integral electron-scattering cross sections, is a good approximation (within 10%) to be used in the energy range considered here (50–10 000 eV). In addition, by comparing our calculated integral elastic cross sections to accurate measurements recently published [23,24], we can consider this method as a reasonable approximation (within 25%) to even around 10 eV. We found that on comparison to BEB results [37], our data suggest that it is a reliable method to describe total electron-impact ionization in THF. Finally, in order to provide data which could be useful to model electron-induced damage in biomolecular systems, an average energy distribution function of secondary electrons generated in THF by incident electron energies from 100 to 5000 eV was also provided.

ACKNOWLEDGMENTS

This study has been partially supported by the following research projects and institutions: Ministerio

de Educación y Ciencia (Plan Nacional de Física, Project No. FIS2006-00702), Consejo de Seguridad Nuclear (CSN), European Science Foundation (COST Action CM0601 and EIPAM Project), Acciones Integradas Hispano-Portuguesas (Project No. HP2006-0042), and the ARC-Center for Antimatter-Matter Studies (CAMS). We acknowledge technical support from the Spanish National Institute for Fusion Research of CIEMAT. One of us (G.G.) also thanks Flinders University for additional support.

[1] S. Gohlke, A. Rosa, E. Illenberger, F. Brüning, and M. A. Huels, J. Chem. Phys. **116**, 10164 (2002).
[2] X. Pan, P. Cloutier, D. Hunting, and L. Sanche, Phys. Rev. Lett. **90**, 208102 (2003).
[3] L. G. Caron and L. Sanche, Phys. Rev. Lett. **91**, 113201 (2003).
[4] S. Trajmar, D. F. Register, and A. Chutjian, Phys. Rep. **97**, 219 (1983).
[5] M. J. Brunger and S. J. Buckman, Phys. Rep. **357**, 215 (2002).
[6] M. Jelisavcic, R. Panajotovic, and S. J. Buckman, Phys. Rev. Lett. **90**, 203201 (2003).
[7] G. García and F. Manero, Phys. Rev. A **53**, 250 (1996).
[8] G. García and F. Manero, Phys. Rev. A **57**, 1069 (1998).
[9] G. García and F. Blanco, Phys. Lett. A **279**, 61 (2001).
[10] G. García, F. Blanco, and A. Williart, Chem. Phys. Lett. **335**, 227 (2001).
[11] F. Blanco and G. García, Phys. Rev. A **67**, 022701 (2003).
[12] F. Blanco and G. García, Phys. Lett. A **317**, 458 (2003).
[13] F. Blanco and G. García, Phys. Lett. A **330**, 230 (2004).
[14] F. Blanco and G. García, Phys. Lett. A **360**, 707 (2007).
[15] F. Blanco and G. García, J. Phys. B **42**, 145203 (2009).
[16] A. Muñoz, J. C. Oller, F. Blanco, J. D. Gorfinkiel, P. Limão-Vieira, and G. García, Phys. Rev. A **76**, 052707 (2007).
[17] H. Landolt and R. Börnstein, *Numerical Data and Functional Relationships in Science and Technology, Group I* (Springer, Berlin, 2003), Vol. 17.
[18] Y. Itikawa and N. Mason, J. Phys. Chem. Ref. Data **34**, 1 (2005).
[19] A. R. Milosavljevic, A. Giuliani, D. Sevic, M.-J. Hubin-Franskin, and B. P. Marinkovic, Eur. Phys. J. D **35**, 411 (2005).
[20] K. Aflatooni, A. M. Scheer, and P. D. Burrow, J. Chem. Phys. **125**, 054301 (2006).
[21] A. Zecca, C. Perazzolli, and M. J. Brunger, J. Phys. B **38**, 2079 (2005).
[22] P. Mozejko, E. Ptasinska-Denga, A. Domaracka, and C. Szmytkowski, Phys. Rev. A **74**, 012708 (2006).
[23] C. J. Colyer, V. Vizcaino, J. P. Sullivan, M. J. Brunger, and S. J. Buckman, New J. Phys. **9**, 41 (2007).
[24] M. Dampc, A. R. Milosavljevic, I. Linert, and M. Zubek, Chem. Phys. Lett. **443**, 17 (2007).
[25] M. Dampc, A. R. Milosavljević, I. Linert, B. P. Marinković, and M. Zubek, Phys. Rev. A **75**, 042710 (2007).
[26] M. Allan, J. Phys. B **40**, 3531 (2007).
[27] C. S. Trevisan, A. E. Orel, and T. N. Rescigno, J. Phys. B **39**, L255 (2006).
[28] D. Bouchiha, J. D. Gorfinkiel, L. G. Caron, and L. Sanche, J. Phys. B **39**, 975 (2006).
[29] C. Winstead and V. McKoy, J. Chem. Phys. **125**, 074302 (2006).
[30] S. Tonzani and C. Greene, J. Chem. Phys. **125**, 094504 (2006).
[31] H. C. Straub, P. Renault, B. G. Lindsay, K. A. Smith, and R. F. Stebbings, Phys. Rev. A **54**, 2146 (1996).
[32] B. L. Schram, F. J. de Heer, M. J. Van der Wiel, and J. Kistemaker, Physica (Amsterdam) **31**, 94 (1965).
[33] D. Rapp and P. Englander-Golden, J. Chem. Phys. **43**, 1464 (1965).
[34] R. R. Goruganthu, W. G. Wilson, and R. A. Bonham, Phys. Rev. A **35**, 540 (1987).
[35] C. B. Opal, E. C. Beaty, and W. K. Peterson, At. Data **4**, 209 (1972).
[36] A. Williart, P. A. Kendall, F. Blanco, P. Tegeder, G. García, and N. J. Mason, Chem. Phys. Lett. **375**, 39 (2003).
[37] P. Mozejko and L. Sanche, Radiat. Phys. Chem. **73**, 77 (2005).